

Real-time observation of the change in light scattering from droplets with increasing deformity

David R Secker, Paul H Kaye, Edwin Hirst

Particle Instruments Research Group, Science and Technology Research Centre

University of Hertfordshire, Hatfield, AL10 9AB, U.K

D.R.Secker@herts.ac.uk

<http://strc.herts.ac.uk/pi/pi.htm>

Abstract: Commercial aerodynamic particle sizing instruments generally achieve the desired particle size measurement by accelerating a sample airstream in which the particles are suspended and measuring the velocity acquired by individual particles. The accelerating flow regime can cause liquid droplets to deform and this subsequently introduces errors. In this paper, we present an apparatus that enables droplet deformation to be observed by recording the spatial light scatter intensity. The paper presents experimental data in video format showing the changes that occur in the light scattering from droplets as a function of increasing flow rate/deformation.

©2001 Optical Society of America

OCIS codes (290.0290) scattering (290.5820) scattering, measurements (290.5850) scattering, particles.

References and links

1. J. K. Agarwal, and R. J. Remiarz, "Development of an aerodynamic particle size analyzer," USDHEW-NIOSH Contract Report No. 210-80-0800, Cincinnati OH: NIOSH (1981).
2. P. A. Baron, "Calibration and use of the Aerodynamic Particle Sizer (APS 3300)," *Aerosol Sci. Technol.* **5**, 55-67 (1986).
3. W. D. Griffiths, P. J. Iles, and N. P. Vaughan, "The behaviour of liquid droplets in an APS 3300," *J. Aerosol Sci.* **17**, 427-431 (1986).
4. S. Holler, Y. Pan, R. K. Chang and J. R. Bottiger, S.C. Hill, D. B. Hillis, "Two-dimensional angular optical scattering for the characterization of airborne microparticles," *Opt. Lett.* **23**, 18, 1489-1491 (1998).
5. E Hirst, P H Kaye, and J R Guppy, "Light scattering from non-spherical airborne particles; theoretical and experimental comparisons," *Appl. Opt.* **33**, (30), 7180-7187 (1994).
6. P.H. Kaye, K. Alexander-Buckley, E. Hirst, and S. Saunders, "A real-time monitoring system for airborne particle shape and size analysis," *J. Geophysical Res. (Atmospheres)*, **101**, D14, 19,215-19,221 (1996).
7. P. H. Kaye, E. Hirst, and Z. Wang-Thomas, "Neural-network based spatial light-scattering instrument for hazardous airborne fiber detection," *Appl. Opt.* **36**, 6149-6156 (1997).
8. C. F. Bohren and D. R. Huffman, *Absorption & Scattering of Light by Small Particles*. (Wiley-InterScience, New York, 1983).
9. Hill, S. C. Benner, R. E., "Morphology-Dependent Resonances" in *Optical Effects Associated with Small Particles*, Barber, P. W. Chang, R. K. eds. (World Scientific Publishing Co., Singapore, 1988).
10. D.R. Secker, P. H. Kaye, R. S. Greenaway, E. Hirst, D. L. Bartley and G. Videen "Light Scattering From Deformed Droplets And Droplets With Inclusions. I: Experimental results," *Appl. Opt.* **39**, 5023-5029 (2000).
11. G. Videen, W. Sun, Q. Fu, D. R. Secker, P. H. Kaye, R. S. Greenaway, E. Hirst, and D.L. Bartley, "Light Scattering From Deformed Droplets And Droplets With Inclusions. II: Theoretical Treatment," *Appl. Opt.* **39**, 5030-5039 (2000).
12. D. L. Bartley, A. B. Martinez, P. A. Baron, D. R. Secker, and E. Hirst, "Droplet Distortion in Accelerating Flow," *J. Aerosol Sci.* **31** 1447-1460 (2000).

1. Introduction

The authors are currently investigating light scattering methods which could be used to correct for the errors that are known to occur in the measurement of liquid droplets by commercial aerodynamic particle sizing instruments. This paper describes the acquisition of experimental light scattering data from deformed droplets. These data may be used to aid the development of instrumentation that could ultimately allow rapid characterization, and/or identification, of these droplet shapes. This in turn could lead to improvements in commercial aerodynamic particle sizers and possible correction of errors when sampling droplets.

1.1 Aerodynamic Particle Sizers

The size of an airborne droplet may be defined in a number of ways depending on the method of measurement. However, in studies of therapeutic aerosol sprays, combustion aerosols, paint sprays and coatings, where on-line or real-time measurements are required and/or where the airborne behavior of the droplet is relevant to the application, the aerodynamic size, d_a , is frequently sought. d_a is defined as the diameter of a unit density sphere having the same gravitational-settling velocity as the particle in question. The traditional method of determining d_a was by measuring the gravitational settling velocity using suitable sedimentation instruments. This process was slow and laborious and commercial instruments based on the acceleration of particles were developed as an alternative [1]. The most widely used commercial aerodynamic sizers are the TSI APS family of instruments (3300 series, TSI Inc., St Paul, MN), which achieve the desired particle size measurement by accelerating a sample airstream in which the particles are suspended and measuring the velocity acquired by individual particles. The larger particles exhibit greater inertia and thus accelerate more slowly, thereby attaining lower velocities. In the APS instruments, an aerodynamic accelerating nozzle, in which a sample flow is sheathed in filtered air, produces the necessary accelerating flow (Fig. 1). The total airflow through the nozzle is regulated to 5.0 l/min, 4.0 l/min of which is filtered to provide the sheath flow. The time-of-flight of the particle through two closely spaced laser beams positioned a few hundred micrometres beneath the nozzle exit is recorded from the pulses of light scattered by the particle to an optical detector. An assessment of the particle's aerodynamic size is determined by relating the transit time to an internal calibration function based upon measured times of flight of solid spherical calibration particles. The size range covered by this instrument is from 0.5 μ m to 30 μ m aerodynamic diameter, depending on the instrument model used.

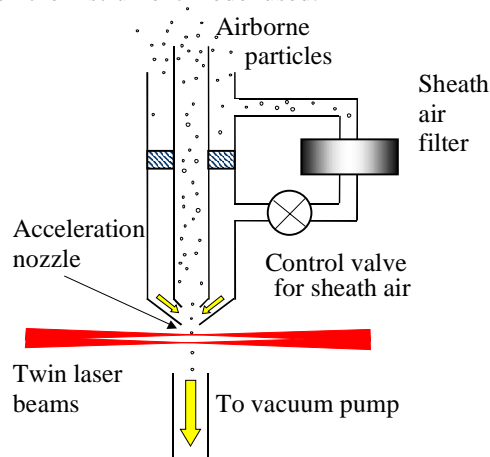


Fig. 1. Schematic diagram of particle delivery system used in TSI Aerodynamic Particle Sizer 3300 series instruments.

However, aerodynamic sizing instruments of this type suffer a significant limitation in that the measured aerodynamic size can be significantly affected by particle shape. When attempting

to measure non-spherical particles of known density, the shape (and orientation) of each particle subjected to the accelerating airflow governs the drag force it experiences and hence affects the measured aerodynamic size. The measurement of liquid aerosol droplets is subject to significant error (25% under-sizing reported in some cases) because the droplets deform to oblate spheroids in the accelerating airflow. Because of this deformation, their cross-sectional area presented to the airflow increases and they experience a greater acceleration than would be the case with similar sized rigid spheres such as polystyrene latex spheres that are used for calibration. Despite being well reported in the past by Baron [2] and Griffiths *et al* [3], there is as yet no systematic method of measuring the degree of deformation experienced by individual droplets in the instrument and material specific calibration curves, derived for example using gravitational settling techniques, are invariably required.

1.2 Spatial Light Scattering

The spatial distribution of light scattered by a particle, referred to as a scattering profile (also in certain texts referred to as a Two-dimensional Angular Optical Scattering (TAOS) pattern [4]), is a complex function of the size, shape, dielectric structure, and orientation of the particle, as well as of the properties of the illuminating radiation (wave-lengths, polarization state). Analysis of the scattering profile can provide a means of characterizing the shape, orientation, and internal structure of the illuminated particle and many workers have exploited this property in various ways. Previous work by the authors [5] has explored the potential of scattering profile analysis for particle shape and size classification and has demonstrated [6,7] how such techniques may be implemented in real-time airborne particle measurement systems designed for ambient aerosol characterization and asbestos fiber detection.

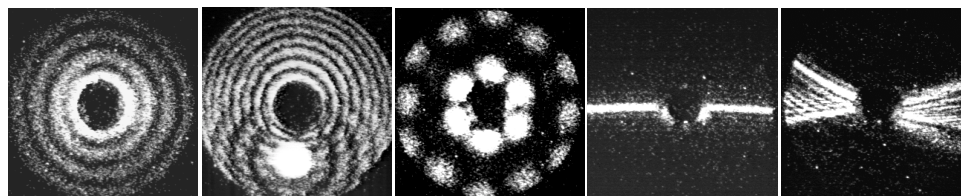


Fig. 2. Examples of spatial light scattering profiles: left to right: 9µm water droplet; 20µm oleic acid droplet with non-concentric water inclusion; sodium chloride crystal; crocidolite fiber; chrysotile fiber.

Scattering profiles can cover different scattering angle ranges depending on the light collection geometry used to acquire them. The examples shown in Fig. 2 were recorded by imaging the transient pattern ($\sim 2\mu\text{s}$ duration) of light scattered by individual particles onto an intensified charge-coupled device (ICCD) camera as the particles are carried by an airstream through a laser beam. Light scattered up to 20° scattering angle relative to the laser beam and around 360° of azimuth passes through a Fourier optic arrangement and captured on the camera. A beam stop placed in the center of the optics cuts out the scattering up to 5° preventing direct illumination of the camera and is the cause of the central dark spot that appears in the images. Each white dot in the profile corresponds to a single scattered photon event and the images thus represent photon distribution maps representing several thousands to several tens of thousands of scattered photons. The images illustrate the wide variations these patterns can assume for different particle shapes and orientations. It was the potential of spatial light scattering analysis for real-time particle shape characterization that initiated the fundamental study of droplet scattering reported here. It also underpins an ultimate aim of this work, namely to provide an on-line optical means of correcting for the errors in measured aerodynamic size caused by droplet deformation in instruments such as the APS3300 series.

2. Experiment

An apparatus was constructed to allow the acquisition of spatial light scattering profiles from individual droplets in the sub-30 μm size range as they traversed the measurement space below an APS3320 sample delivery nozzle (donated by TSI Inc.). The apparatus is shown schematically in Figure 3. As stated above, the actual TSI APS3300 series of instruments incorporate two closely spaced cross-polarized beams and measure particle time-of-flight between the beams. However, for the fundamental results reported here the spatial light scattering profile images were produced using a single beam from a 633nm 15mW plane polarized Helium-Neon laser. The normal operating flow-rate of the TSI APS instrument is 5.0 l/min (comprising 1.0 l/min sample flow-rate and 4.0 l/min of filtered sheath flow). In this work we have additionally observed droplet behavior over a range of flow conditions both less than and greater than the norm to gain a greater understanding of the morphological changes taking place.

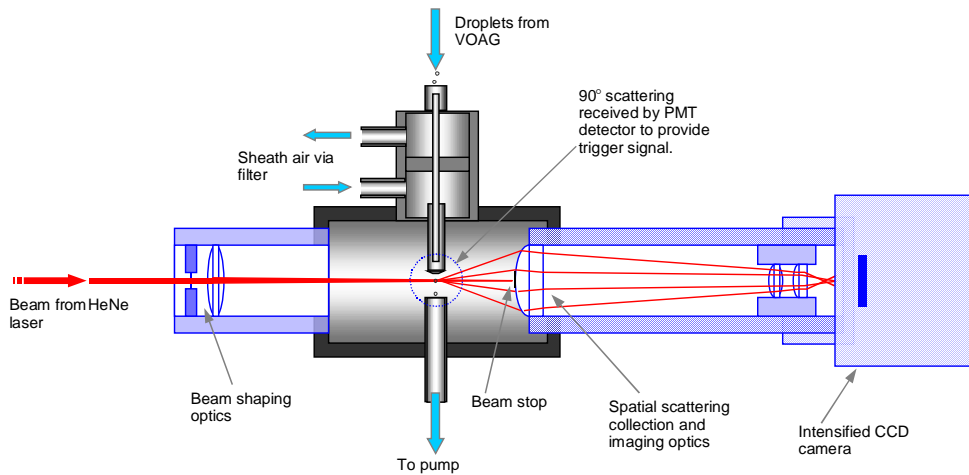


Fig. 3 Schematic diagram showing apparatus used to investigate droplet deformation.

2.1 Light Scattering Profile Acquisition

The beam from the HeNe laser passes through a quarter-wave plate to render the light circularly polarized before being focused by a cylindrical lens to produce a beam of elliptical cross-section (approximately 1.2mm by 100 μm) at the point of intersection with the sample airflow. Monodisperse droplets are generated into the sample flow using a Vibrating Orifice Aerosol Generator, VOAG (TSI Inc., St. Paul, MN) as described below. As each droplet traverses the beam, light scattered in the forward direction between angles of 5° and 20° passes through the Fourier optic and onto the faceplate of the intensified, asynchronously triggered ICCD camera. The lower angular limit is set by the beam-stop, whilst the higher limit is set to avoid shadowing of the scattered light by the lower surface of the sample delivery nozzle. Images from the camera are digitized, displayed, and stored on a computer at a rate of several images per second for later analysis. A trigger signal for the acquisition of a scattering profile by the camera is derived from a separate photomultiplier detector module that receives light scattered at a higher scattering angle than the camera, as indicated in Figure 3. The rising and trailing edges of the signal from the photomultiplier detector initiate and terminate the camera integration period respectively, this being typically $\sim 2\mu\text{s}$ duration.

The VOAG produces monodisperse droplets by inducing mechanical instability in a fine liquid jet through excitation with a piezo-electric oscillator. When first formed droplets are comparatively large and comprise a solute, in this case di-ethyl phthalate (DEP), in solution with AR grade *iso*-propyl alcohol. Dry (<1%RH) compressed air is used to transport the droplet aerosol from the VOAG drying column to the light scattering instrument, during which time the alcohol evaporates to leave smaller pure DEP droplets. A bleed valve controls the total flow-rate through the nozzle subsystem. The total flow comprises the sheath and sample flow-rate in the ratio 4:1 respectively. This ratio remained constant throughout the experimentation. In order to observe the changes in light scattering that occurs due to droplet deformation the total flow-rate, and hence the shear force experienced by the droplets was varied; The total flow rate was set to 1.0 l/min prior to the experiment and was increased from 1.0 l/min to 6.0 l/min throughout the acquisition of scattering data which lasted approximately 30 seconds.

3. Results

All the experimental data presented here were recorded from di-ethyl phthalate droplets that are nominally 20 μ m in diameter. The video file showing the effect of increasing flow rate on the scattering profiles from droplets is given in fig. 4.

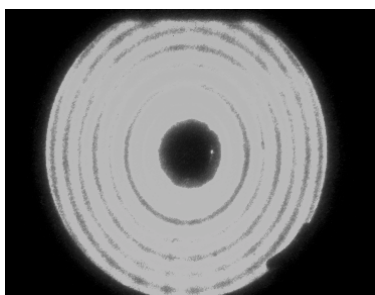


Fig. 4. (3.1MB) Movie showing spatial light scattering profiles of di-ethyl-phthalate showing increasing deformation with increasing sample flow rate from 1.0 l/min to 6.0 l/min.

The sequence observed in figure 4 is: concentric rings turning into concentric ellipses; then a high intensity horizontal band across the center; then horizontal fringes; then radial fringes; and finally a high intensity vertical band down the center. This sequence is a result of increasing droplet deformation.

4. Discussion

In attempting to gain knowledge of the morphological changes taking place due to the increasing droplet deformation in an accelerating flow field, an apparatus was constructed to record the spatial scattering from individual droplets in the flow. The experimental data presented in this paper illustrate the complex spatial light scattering behavior of droplets distorted by accelerating flow fields. The reproducibility of the experimental data makes them a valuable resource in the development of instrumentation for the rapid characterization and/or identification of complex droplet morphologies, and this in turn could lead to advances in instrumentation for droplet aerodynamic sizing. When the particle is spherical, the profiles show the concentric ring pattern as predicted by Mie theory. As the droplets deform into oblate spheroids, the concentric rings become concentric ellipses, whose semi-major axis is orthogonal to the semi-major axis of the oblate spheroid. With increased deformation, the scattering exhibits a high intensity horizontal band. This band is hypothesized as being a result of a morphology dependent resonance (MDR)[9]. Further deformation results in the high intensity horizontal band splitting into horizontal fringes. Further increases in flow rate leads

to the horizontal fringes being replaced with radial fringing and subsequently a high intensity vertical band. This same sequence has been observed for other droplets that have different surface tension and viscosities (e.g. oleic acid, glycerine). Consequently, analysis of this sequence could give the ability to correct for droplet deformation on-line. The top row of figure 5 shows individual light scattering profiles from the same nominal size droplets; the bottom row shows the corresponding images (acquired using apparatus described elsewhere [10]) and shows the droplet morphologies that produced that type of scattering.

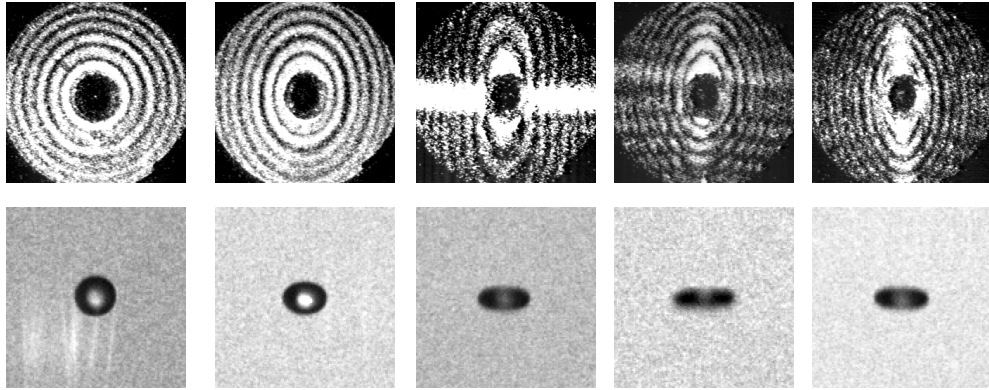


Fig. 5. Top row, light scattering patterns from deformed droplets; Bottom row, images of the droplets corresponding to the same experimental conditions.

More detailed experimental data on different droplet sizes (and their corresponding images) of deformed droplets during measurement, and the theoretical treatment of their light scattering is given elsewhere [10,11]. Analytical derivation of droplet deformation and correlation with the experimental data reported here has been the subject of recent work by Bartley *et al.* [12].

Acknowledgements: This work was carried out with funding from the UK Engineering and Physical Sciences Research Council with support from TSI Inc. St. Paul. MN.